Clinical Pharmacology
in Drug Development
2020, 9(6) 689–698

DOI: 10.1002/cpdd.784

# Modeling and Simulation of the Pharmacokinetics and Target Engagement of an Antagonist Monoclonal Antibody to Interferon-$\gamma$–Induced Protein 10, BMS-986184, in Healthy Participants to Guide Therapeutic Dosing

**Weiguo Cai[1], Tarek A. Leil[1], Leonid Gibiansky[2], Murli Krishna[1], Hongwei Zhang[1], Huidong Gu[1], Huadong Sun[1,*], John Throup[1], Subhashis Banerjee[1], and Ihab Girgis[1]**

**Abstract**

BMS-986184 is a human, second-generation, anti–interferon-$\gamma$–induced protein 10 (IP-10) monoclonal antibody. In this study the pharmacokinetics and target engagement (TE) of BMS-986184 in healthy participants were characterized using population-based target-mediated drug disposition (TMDD) modeling and data from a first-in-human study (NCT02864264). The results of the first-in-human study and the model generated were used to conduct stochastic simulations of a virtual population of healthy participants to predict pharmacokinetic exposures and TE responses for different dosage regimens. A 2-compartment, 2-target, TMDD structural model, assuming quasi-steady-state and stimulated production on treatment, was developed by simultaneous fitting of the total drug, serum-free IP-10, and serum total IP-10 concentration data, with the second unobservable target contribution to drug elimination described by the Michaelis-Menten elimination term. Model evaluation confirmed agreement between model predictions and observed data. Simulation of a virtual population of healthy individuals demonstrated that steady state was reached at the eighth dosing interval, and that around 150 mg subcutaneously every other week could be a suitable target dosage regimen for future clinical trials. Integrated modeling strategies such as this can be used to help guide rational clinical trial development of drugs with TMDD, leading to improved dose selection and greater patient benefits.

**Keywords**

monoclonal antibody, target-mediated drug disposition, pharmacokinetics, simulation, IP-10

Interferon (IFN)-$\gamma$-induced protein 10 (IP-10/CXC motif chemokine [CXCL]10), a member of the CXC chemokine family, is involved in a diverse range of human diseases, including inflammatory and autoimmune diseases (eg, rheumatoid arthritis,[1] systemic lupus erythematosus,[2] and type 1 diabetes mellitus[3]) and cancer.[4-6] IP-10 is secreted by immune cells (lymphocytes,[7] eosinophils,[8] and monocytes[9]) and nonimmune cells (hepatocytes,[7] endothelial cells,[9] fibroblasts,[9] stromal cells,[10] and keratinocytes[9]) in response to inflammatory stimuli,[6,11] and its production is significantly increased in the circulation and diseased tissues of patients with several autoimmune diseases.[12,13] Experimental models of ulcerative colitis (UC) have demonstrated that IP-10 mediates the trafficking of immune cells from the circulation to the inflamed colon[14] and regulates crypt cell proliferation.[15] In addition, IP-10 has the ability to induce proinflammatory cytokine production by IFN-$\gamma$–primed human

[1] Bristol-Myers Squibb, Princeton, New Jersey, USA
[2] QuantPharm LLC, North Potomac, Maryland, USA



Submitted for publication 19 August 2019; accepted 12 January 2020.

**Corresponding Author:**
Ihab Girgis, Bristol-Myers Squibb, Princeton, NJ 08540
(e-mail: ihab.girgis@bms.com)

*Address at the time of analysis.

monocytes.[16] Inhibiting IP-10 activity with a therapeutic monoclonal antibody (mAb) has demonstrated some evidence of efficacy in patients with moderate to severe UC, as shown in a phase 2 clinical trial with a first-generation anti–IP-10 antagonist antibody, eldelumab.[12] BMS-986184 is a second-generation anti–IP-10 neutralizing mAb with higher affinity and potency than eldelumab.[12] In binding assays, BMS-986184 binds to human IP-10 with a dissociation constant ($K_D$) of <0.1 nmol/L.

A large proportion of mAbs have nonlinear pharmacokinetics (PK) that are dependent on their structures as well as on the expression and biology of the target antigen, typically displaying target-mediated drug disposition (TMDD, defined as a drug binding with such a high affinity to its pharmacological target site that this binding affects its PK characteristics).[17] Therefore, effective PK characterization of such mAbs can be difficult but is still essential to facilitate selection of a dose and dosage regimen that optimize therapeutic efficacy and safety. An efficient dose selection for mAbs seeks to provide adequate exposure in all treated patients.[18] Strategies such as flat dosing and variable dosing based on body weight must be supported by PK characterization, including information on TMDD and target engagement (TE).[18] Therefore, population PK and pharmacodynamic (PD) model-based approaches are typically used to characterize the PK and PD of mAbs to facilitate dose selection of such agents.[18,19]

The system of equations representing the free drug, the target, and the drug-target complex in TMDD models provides a framework that allows for the quantification of biological processes and is frequently used to characterize the PK of mAbs. In practice the use of the full TMDD models to describe population PK and PD is most successful when the drug concentration, target concentration, and drug-target complex concentrations are all available and adequately sampled. However, with the complexity of TMDD models and the frequently sparsely sampled data in clinical trials, it is often not feasible to fit the full TMDD models. Difficulties may arise in the attempt to identify model parameters based on available data, as detailed information regarding the time scale of drug-target association processes is required.[20] Many TMDD models have been widely used in research to characterize TE and interactions between a mAb and soluble targets,[21-23] and a thorough review has been written about the various TMDD models and their applications.[24] Several simpler approximations of the full TMDD models have been developed to fit data more feasibly: the quasiequilibrium model,[25] the quasi-steady-state (QSS) model,[26] and the Michaelis-Menten (MM) model.[26]

With the unique PK of these mAbs in mind, the primary objectives of this study were to characterize the PK and TE of BMS-986184 in healthy participants using population-based TMDD modeling in a first-in-human (FIH) study of BMS-986184. We applied the model results to conduct stochastic simulations of a virtual population of healthy participants to predict PK exposures and TE responses for different dosage regimens.

## Methods

### Study Design

A FIH, double-blind, randomized, single ascending dose (SAD) and multiple ascending dose (MAD) study (IM012-004; NCT02864264) was conducted to evaluate an anti–IP-10 neutralizing mAb, BMS-986184, for its safety, PK, and activity for inhibiting IP-10 in healthy participants. The first stage of the study consisted of 7 single-dose panels: 30 mg intravenously (IV), 37.5 mg IV, 100 mg IV, 200 mg IV, 300 mg IV, 100 mg subcutaneously (SC), and 200 mg SC. The second stage consisted of 2 IV MAD panels (75 mg and 200 mg with once every 2 weeks [Q2W] dosing for 2 doses). Population PK, free IP-10, total IP-10, and target concentration data in serum were obtained with actual sampling times. The scheduled PK sampling times relative to dosing were 0, 0.5, 1, 2, 6, 12, 24, 48, 72, 120, 168, 240, 336, 504, 672, 1008, and 1344 hours, and the scheduled serum free and total IP-10 sampling times relative to dosing were 0, 6, 24, 72, 168, 336, 504, 672, and 1344 hours. A total of 72 participants were included in this study (Table 1); in each panel, 6 participants were administered BMS-986184, and a total of 18 participants received placebo in a blinded manner. The protocol, any amendments, and the participants' written informed consent received approval by Nucleus Network Limited, Centre for Clinical Studies (Melbourne, Australia) and regulatory authorities according to applicable local regulations before initiation of the study.

### Bioanalytical Methods

An electrochemiluminescent assay was used to quantify the levels of BMS-986184 in human serum. Meso-Scale Discovery (Rockville, Maryland) streptavidin-coated plates were first coated with biotinylated mouse mAb specific to BMS-986184 clone 1674.5174.1B9.D11.F9 to capture the test analyte from samples. Samples, calibrators, and controls were diluted to a minimum required dilution of 80-fold in assay buffer and added to the wells. The captured BMS-986184 was detected using ruthenium trisbipyridine-labeled mouse mAb specific to BMS-986184 clone 1673.5173.11G9.H8.C6.

**Table 1.** Baseline Demographics of the SAD and MAD Data Sets

| | SAD | | | | | | | | MAD | | |
|---|---|---|---|---|---|---|---|---|---|---|---|
| | Placebo n = 14 | 30 mg IV n = 6 | 37.5 mg IV n = 6 | 100 mg IV n = 6 | 200 mg IV n = 6 | 300 mg IV n = 6 | 100 mg SC n = 6 | 200 mg SC n = 6 | Placebo n = 4 | 75 mg IV n = 6 | 200 mg IV n = 6 |
| Age (y)[a] | | | | | | | | | | | |
| Mean | 27.4 | 26.0 | 27.2 | 25.7 | 23.0 | 26.8 | 26.3 | 27.5 | 26.5 | 29.0 | 33.5 |
| Median | 28.0 | 27.0 | 28.0 | 27.0 | 22.0 | 27.0 | 26.5 | 25.5 | 26.0 | 25.0 | 32.0 |
| Min, max | 19, 41 | 19, 33 | 20, 30 | 18, 34 | 19, 31 | 22, 31 | 19, 33 | 23, 41 | 24, 30 | 22, 51 | 26, 45 |
| SD | 5.15 | 5.93 | 3.71 | 6.59 | 4.34 | 3.49 | 4.97 | 6.80 | 2.52 | 11.15 | 6.63 |
| Female, n (%) | 4 (28.6) | 2 (33.3) | 2 (33.3) | 4 (66.7) | 1 (16.7) | 2 (33.3) | 3 (50.0) | 2 (33.3) | 2 (50.0) | 0 | 0 |
| Race/ethnicity, n (%) | | | | | | | | | | | |
| White | 13 (92.9) | 4 (66.7) | 5 (83.3) | 4 (66.7) | 6 (100.0) | 5 (83.3) | 5 (83.3) | 3 (50.0) | 3 (75.0) | 6 (100.0) | 5 (83.3) |
| Asian Indian | 0 | 1 (16.7) | 0 | 0 | 0 | 0 | 0 | 0 | 0 | 0 | 0 |
| Asian Chinese | 0 | 0 | 0 | 1 (16.7) | 0 | 1 (16.7) | 0 | 1 (16.7) | 0 | 0 | 0 |
| Asian other | 0 | 1 (16.7) | 1 (16.7) | 0 | 0 | 0 | 1 (16.7) | 0 | 0 | 0 | 1 (16.7) |
| Other | 1 (7.1) | 0 | 0 | 1 (16.7) | 0 | 0 | 0 | 2 (33.3) | 1 (25.0) | 0 | 0 |

IV indicates intravenously; MAD, multiple ascending dose; SAD, single ascending dose; SC, subcutaneously; SD, standard deviation.
[a]All participants were <65 years of age.

After the addition of tripropylamine-based read buffer, the plate was read by an MSD 2400 plate reader that energized electrodes built into the bottom of the plate, causing the ruthenium trisbipyridine label to produce a chemiluminescent signal. The measured electrochemiluminescent signal (ie, relative light units) was proportional to the amount of antibody component of BMS-986184 in the sample. The lower limit of quantification (LLOQ) of the assay was 0.67 nmol/L (100 ng/mL). The average precision and bias calculated from all the runs are within acceptance criteria established during method validation of the PK assay.

Free and total IP-10 (free plus IP-10 complexed with antibody) were measured in human serum samples with 2 different immunocapture–liquid chromatography–tandem mass spectrometry assays. A competing anti–IP-10 mAb, immobilized on protein G magnetic beads, was used as the capture antibody for free IP-10, and a biotinylated noncompeting anti–IP-10 antibody immobilized on streptavidin magnetic beads was used as the capture antibody for total IP-10. Samples were eluted from the magnetic beads followed by thermal denaturation and trypsin digestion. Analysis of the surrogate peptide with multiple reaction monitoring transition (m/z) of 452.8 to 676.4 was carried out on a Sciex (Framingham, Massachusetts) Triple Quad 6500 system coupled with a Shimadzu (Kyoto, Japan) ultraperformance liquid chromatography system. Analytical runs used appropriate calibration curves and quality control samples that met the preestablished acceptance criteria. The LLOQ of the free IP-10 assay was 0.0012 nmol/L (10 pg/mL), and the LLOQ of the total IP-10 assay was 0.012 nmol/L (100 pg/mL).

## Software Used for Analysis

The population PK/PD analyses and simulation were performed using NONlinear Mixed Effect Modeling (NONMEM) software (Icon plc, Dublin, Ireland; Version 7.3). Exploratory analyses, presentations of the data, diagnostic graphics, and postprocessing of NONMEM outputs were performed using R software (R Foundation, Vienna, Austria; Version 3.3.1).

## Model Development

*Model Selection.* Model selection was primarily guided by biologic considerations, diagnostic plots, and objective function value. Bayesian information criterion values were used for model comparisons (Table S1). Initially, a TMDD structural model with QSS assumption was used to describe BMS-986184, free IP-10, and total IP-10 concentrations. QSS assumption is used when the binding rate of the drug to the receptor is balanced by the sum of the dissociation and internalization rates; the dissociation rate constant $K_{off}$ is replaced by the sum of $K_{off}$ and the internalization rate constant $K_{int}$ in the expression for the dissociation constant $K_{SS}$.[26] SC administration was described by the first-order absorption process. Log-normal distribution of all random effects and combined additive and proportional residual error model (for each analyte) were used. To allow simultaneous fit of data from all analytes, dose and observed concentration data were converted to molar units. The QSS model was the best among many other tested models, from the 2-compartment linear model to different complex TMDD models. Model diagnostics revealed dose dependencies of the model parameters. To improve the fit, a MM elimination term was added,

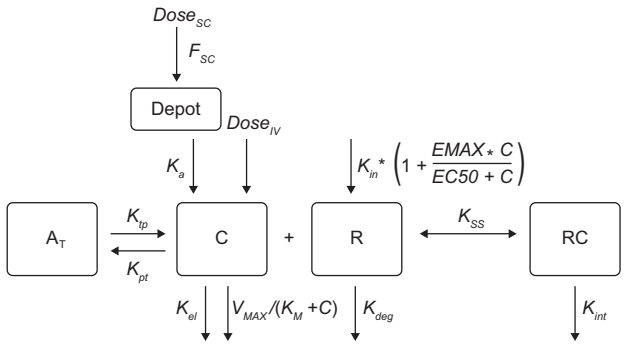


$$C_{tot} = \frac{A_2}{V_c}$$

$$C = 0.5 * \left[ (C_{tot} - A_4 - K_{ss}) + \sqrt{(C_{tot} - A_4 - K_{ss})^2 + 4 * K_{ss} * C_{tot}} \right]$$

$$\frac{dA_1}{dt} = -K_a * A_1$$

$$\frac{dA_2}{dt} = K_a * A_1 - \frac{K_{int} * A_4 * C * V_c}{K_{ss} + C} - (K_{el} + K_{pt}) * C * V_c + K_{tp} * A_3 - \frac{V_{MAX} * A_2}{K_M + C}$$

$$\frac{dA_3}{dt} = K_{pt} * C * V_c - K_{tp} * A_3$$

$$\frac{dA_4}{dt} = K_{in} * \left(1 + \frac{EMAX * C}{EC50 + C}\right) - K_{deg} * A_4 - (K_{int} - K_{deg}) * \frac{A_4 * C}{K_{ss} + C}$$

$$A_1(t=0) = 0;\ A_2(t=0) = 0;\ A_3(t=0) = 0;\ A_4(t=0) = \frac{K_{in}}{K_{deg}}$$

**Figure 1.** TMDD final model with stimulation of production. The drug (C) in the central compartment was assumed to have first-order elimination ($K_{el}$) and an extra nonspecific nonlinear clearance with the Michaelis-Menten model ($V_{MAX}/[K_m+C]$) used to model this process. The drug was also assumed to be distributed to and from peripheral tissue compartment ($A_T$) by first-order rates ($K_{pt}$ and $K_{tp}$). In addition, the drug in the central compartment was assumed to have a target-mediated process with free IP-10 target (R). R was assumed to be degraded with rate $K_{deg}$. The quasi-steady-state model was used to model the process with $K_{SS}$ as the dissociation constant. The drug and IP-10 target complex (RC) was assumed to either dissociate or be degraded by the internalization process ($K_{int}$). The EMAX function EMAX*C/(EC50+C) was added as the additional coefficient for $K_{in}$, which represents the stimulation of the free IP-10 target production by the drug concentration. IP-10, interferon-$\gamma$–induced protein 10.

converting the standard TMDD QSS model to the TMDD QSS 2-target model.[27] These terms could be responsible for the elimination of the drug by binding to the monokine induced by IFN-$\gamma$ (MIG/CXCL9 target) in addition to IP-10. Even the TMDD QSS 2-target model did not capture the peaks of total IP-10 targets following peaks of total drug well. Attempts to introduce an additional distribution compartment for total IP-10 were not successful, but the fit significantly improved when stimulation of the IP-10 production by the drug was added to the model.

*Estimation Methodology.* Initially, the first-order conditional estimation with interaction (FOCEI) method in NONMEM was used to estimate nonlinear mixed-effects model parameters in model development, a method typically used when the observed data are normally distributed.[28] In the later stages of model development the NONMEM Monte Carlo expectation-maximization method with importance sampling was implemented due to the difficulty of obtaining convergence of the FOCEI method with increasing complexity of the model. Unlike FOCEI, the expectation-maximization method with importance sampling method works best when each structural parameter of the model is associated with the random effect. Therefore, random effects were included for all structural parameters.[28] To describe observations below the quantification limit, the M3 method[29] was used to maximize the likelihood for all the data, treating data below the quantification limit as left-censored observations (ie, the value is not known, but it is known to be below the quantification limit of the assay).

### Model Evaluation

Diagnostic plots and visual predictive checks were carried out to evaluate the model fit and confirm the predictive quality of the model.

### Model Application

Simulations were conducted using the final TMDD model to predict the PK and PD profiles of BMS-986184 in a virtual population of healthy participants. Simulations were carried out for the 6 SC Q2W dose panels, with each dose panel represented by a typical individual in the simulation. Simulations were run 1000 times for 25 dose intervals for each dose panel. Simulations were also used to evaluate relative contributions of nonspecific linear, IP-10–mediated, and, hypothetically, MIG/CXCL9-mediated elimination pathways.

## Results

### Study Population

In total, 54 healthy participants who received BMS-986184 were included in the analysis data set for the model development. The analysis data set included 744 PK concentration observations, 523 free IP-10 concentration observations, and 523 total IP-10 concentration observations. Overall, 348 free IP-10 concentration observations (66.5%) from 54 participants and 21 total IP-10 concentration observations (4.0%) from 20 participants were below the LLOQ in the analysis data set.

Overall, 35/42 (83.3%) participants who received BMS-986184 in the SAD study and 8/12 (66.7%) participants who received BMS-986184 in the MAD study completed the study period. The main reasons for not

**Table 2.** Parameter Estimates for Final TMDD Model

| Parameter[a] | Symbol | Estimate | RSE, % | 95% CI[b] |
|---|---|---|---|---|
| Fixed effects | | | | |
| CL (L/h) | $\exp(\theta_1)$ | 0.021 | 61.1 | 0.006-0.07 |
| $V_C$ (L) | $\exp(\theta_2)$ | 3.521 | 5.3 | 3.177-3.903 |
| Q (L/h) | $\exp(\theta_3)$ | 0.031 | 49.5 | 0.012-0.081 |
| $V_P$ (L) | $\exp(\theta_4)$ | 3.255 | 20.7 | 2.168-4.886 |
| $K_a$ (1/h) | $\exp(\theta_5)$ | 0.009 | 32.4 | 0.005-0.017 |
| $K_{in}$ (nmol/[Lh]) | $\exp(\theta_6)$ | 0.020 | 28.4 | 0.011-0.034 |
| $K_{deg}$ (1/h) | $\exp(\theta_7)$ | 1.247 | 39.7 | 0.573-2.714 |
| $K_{int}$ (1/h) | $\exp(\theta_8)$ | 0.109 | 21.5 | 0.071-0.166 |
| $K_{SS}$ (nmol/L) | $\exp(\theta_9)$ | 0.002 | 77.2 | 0.001-0.011 |
| F1 | $\exp(\theta_{10})$ | 0.787 | 37.5 | 0.377-1.643 |
| EMAX | $\exp(\theta_{11})$ | 6.367 | 36.8 | 3.093-13.11 |
| EC50 (nmol/L) | $\exp(\theta_{12})$ | 96.57 | 165.1 | 3.797-2456 |
| $V_{MAX}$ (nmol/[Lh]) | $\exp(\theta_{13})$ | 0.146 | 13.5 | 0.112-0.19 |
| $K_m$ (nmol/L) | $\exp(\theta_{14})$ | 2.886 | 13.2 | 2.229-3.737 |
| $T_{½}$ (h)[c] | | 264.5 | | |
| Random effects | | | | |
| $\omega^2_{CL}$ | $\Omega(1, 1)$ | 0.419 | 93.6 | 0-1.188 |
| $\omega^2_{V_C}$ | $\Omega(2, 2)$ | 0.036 | 73.6 | 0-0.088 |
| $\omega^2_{Q}$ | $\Omega(3, 3)$ | 0.769 | 39.1 | 0.18-1.358 |
| $\omega^2_{V_P}$ | $\Omega(4, 4)$ | 0.492 | 18.6 | 0.313-0.671 |
| $\omega^2_{K_a}$ | $\Omega(5, 5)$ | 0.181 | 58.2 | 0-0.387 |
| $\omega^2_{K_{in}}$ | $\Omega(6, 6)$ | 0.117 | 30.1 | 0.048-0.186 |
| $\omega^2_{K_{deg}}$ | $\Omega(7, 7)$ | 0.031 | 354.3 | 0-0.249 |
| $\omega^2_{K_{int}}$ | $\Omega(8, 8)$ | 0.034 | 120.3 | 0-0.115 |
| $\omega^2_{K_{SS}}$ | $\Omega(9, 9)$ | 3.181 | 58.0 | 0-6.794 |
| $\omega^2_{F1}$ | $\Omega(10, 10)$ | 0.260 | 139.6 | 0-0.97 |
| $\omega^2_{EMAX}$ | $\Omega(11, 11)$ | 0.347 | 170.1 | 0-1.502 |
| $\omega^2_{EC50}$ | $\Omega(12, 12)$ | 3.503 | 49.4 | 0.114-6.893 |
| $\omega^2_{V_{MAX}}$* | $\Omega(13, 13)$ | 0.010 | | |
| $\omega^2_{K_M}$* | $\Omega(14, 14)$ | 0.010 | | |
| Residual error | | | | |
| $\sigma^2_{p\_drug}$ | $\Sigma(1, 1)$ | 0.040 | 5.0 | 0.036-0.044 |
| $\sigma^2_{a\_drug}$ | $\Sigma(2, 2)$ | 0.559 | 73.4 | 0-1.364 |
| $\sigma^2_{p\_free\_ip10}$ | $\theta_{15}$ | 0.433 | 15.9 | 0.299-0.568 |
| $\sigma^2_{a\_free\_ip10}$ | $\theta_{16}$ | 0.000 | 16.5 | 0-0.001 |
| $\sigma^2_{p\_total\_ip10}$ | $\theta_{17}$ | 0.369 | 9.6 | 0.299-0.439 |
| $\sigma^2_{a\_total\_ip10}$ | $\theta_{18}$ | 0.007 | 18.4 | 0.005-0.01 |

CL indicates clearance; EC50, drug concentration to achieve 50% of EMAX; EMAX, maximum percentage of the stimulation of the free IP-10 target production by the drug concentration; F1, bioavailability constant; IP-10, interferon-$\gamma$–induced protein 10; $K_a$, absorption rate; $K_{deg}$, free IP-10 target degradation rate; $K_{in}$, free IP-10 target production rate; $K_{int}$, elimination rate constant of the drug–target complex; $K_m$, Michaelis-Menten constant of target-mediated drug elimination from the central compartment; $K_{SS}$, dissociation constant of the drug-target complex; $\omega^2_{Par}$, variance of the random effects on parameter Par (Par = CL, $V_C$, Q, $V_P$, $K_a$, $K_{in}$, $K_{deg}$, $K_{int}$, $K_{SS}$, F1, EMAX, EC50, $V_{MAX}$, $K_M$); Q, intercompartment clearance; RSE, relative standard error; $\sigma^2_{p\_Dat}$ and $\sigma^2_{a\_Dat}$, the proportional and additive residual error variance correspondingly for the Dat (Dat = drug, free IP-10, and total IP-10); $T_{½}$, elimination half-life; TMDD, target-mediated drug disposition; $V_C$, volume of the central compartment; $V_{MAX}$, maximum target-mediated drug elimination rate from the central compartment in Michaelis-Menten function; $V_P$, volume of the peripheral compartment.

[a]Parameter with fixed values (not estimated) are denoted with an * after the names, with the fixed value given in the Estimate column.

[b]Confidence intervals of fixed effects are obtained by exponentiating the estimated confidence intervals for the corresponding parameter $\theta$. Confidence interval of random effects and residual error parameters are for variance.

[c]Computed as $\beta$ half-life. Shows the half-life of a linear part of the model, valid at high concentrations when nonlinear elimination is small relative to the linear part.

completing the study were withdrawal of consent (3/54; 5.6%) and adverse events (AEs; 3/54; 5.6%). Baseline characteristics for both the SAD and MAD cohorts are shown in Table 1.

## Final Model

Among all tested models, QSS approximation of the 2-target TMDD model with stimulation of IP-10 production (Figure 1) had the lowest Bayesian information criterion. Therefore, it was chosen as the final model for the analysis. Parameter estimates for this model are shown in Table 2.

## Model Fitting and Estimation

Visual predictive checks confirmed the good fit of the model (Figure S1). Diagnostic plots of the final model demonstrated reasonable estimates of fixed (Figure S2) and random (Figure S3) parameters. Plots of observed versus predicted values for drug concentration (Figure S4A), free IP-10 concentration (Figure S4B), and total IP-10 concentration (Figure S4C) demonstrated that the observed versus predicted concentrations were aligned around the 45° line. There were no obvious trends in the plots of normalized probability distribution errors versus time or dose (Figure 2). In addition, visualizations of the concentration data (drug, free IP-10, and total IP-10) were plotted for each patient in each of the 9 dose panels with predicted lines from the model (Figure S5). The final TMDD structural model, with QSS assumption and stimulation of production, fit reasonably well for the drug, free IP-10, and total IP-10 concentration data across all doses studied. NONMEM codes for the final model are shown in the supplementary materials.

## Model Application

The median trough concentration ($C_{min}$) at the seventh dose interval varied from 0 to 1.4% of the $C_{min}$ at the eighth dose interval for all 6 dose panels in the

simulation. The median $C_{min}$ at the eighth dose interval varied by less than 1% of the $C_{min}$ at the ninth dose interval for all 6 dose panels in the simulation. Therefore, 99% steady state was reached at the eighth dose. To be conservative, the 25th dose interval (8400 hours) was chosen as the PK steady state for the summary.

Drug (Figure S6A), free IP-10 (Figure S6B), and total IP-10 (Figure S6C) concentration profiles from simulation were summarized for steady state. With a 2-week dosing interval, suppression of free IP-10 was observed across all doses studied, with a greater duration of suppression seen with increasing doses. The shape of the total IP-10 curve is similar to that of the drug's PK profile; increases in total IP-10 appear to reflect increases in drug concentration. Nonlinear, dose-dependent increases in $C_{min}$, maximum concentration, average concentration, and area under the concentration–time curve within the Q2W interval were seen (Figure 3), with a visible plateau observed with a dose of 150 mg.

Plots of free IP-10 percentage as baseline values (median and 5% and 95% quantiles) were generated. With a dose of 150 mg (Figure S7) for the majority of the dosing interval (ie, 2 weeks), the 95% quantiles of IP-10 as a percentage of baseline value were below 10% (believed to be effective target suppression). Free IP-10 as a percentage of baseline value at steady state for all doses is shown in Figure 4; for doses ≥100 mg, free IP-10 as a percentage of the baseline value at steady state was maintained at ~0% over the 2-week dosing interval; with doses ≥150 mg, the 95% quantile of free IP-10 as percentages of baseline values were almost all within 10%. Free IP-10 summary exposure parameters at steady state are shown in Figure 5. Decreases in free IP-10 concentrations were seen with increasing drug doses, as with the plots of drug exposure parameters, and a plateau was seen close to 150 mg. Simulation with every-4-week multiple-dose panels produced similar results to that of the Q2W dose panel, indicating that dosing in this schedule may be feasible (data not shown). Table 3 presents relative fractions of the dose eliminated by 3 different elimination pathways (linear, IP-10–mediated, and MM-mediated) at steady state for different dose levels, computed as median over 1000 simulated participants at each dose level.

## *Safety*

In total, 78.6% of participants who received BMS-986184 and 71.4% who received placebo in the SAD study experienced an AE (Table S2). In the MAD study 100% of the patients in each treatment group reported AEs (Table S3). No deaths were reported in either study, and there were no dose-related trends in the incidence or severity of AEs. There were no serious AEs (SAEs) or discontinuations due to AEs

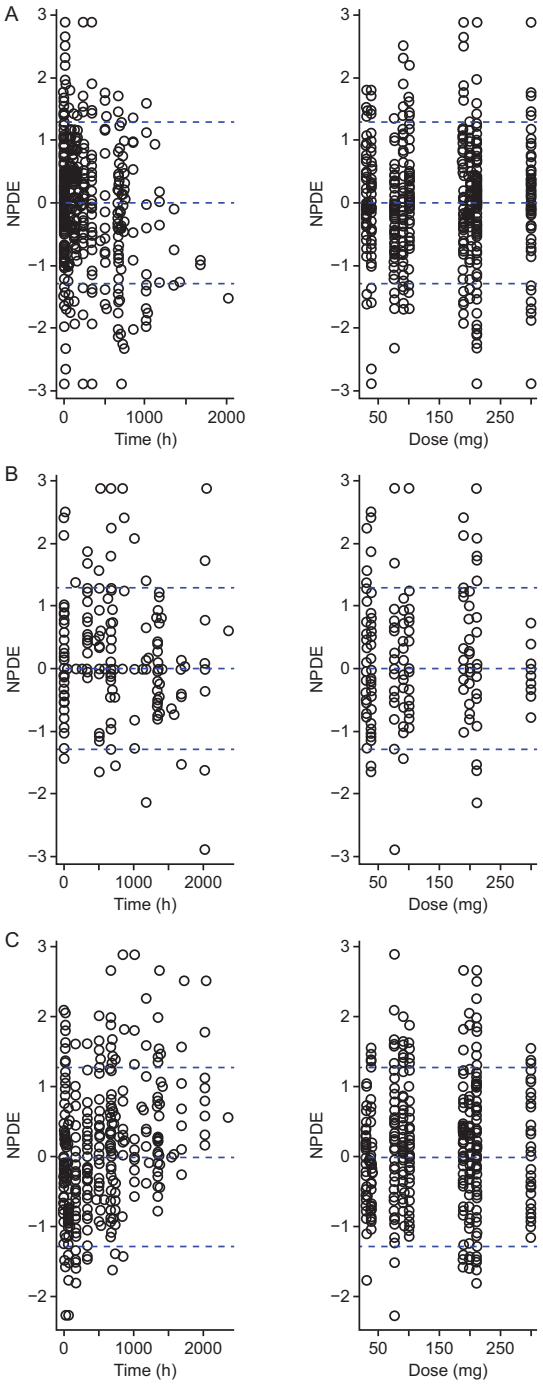


**Figure 2.** Normalized probability distribution error for (A) drug concentration, (B) free IP-10 concentration, and (C) total IP-10 concentration. The 3 dashed lines in each panel represent the expected 10th percentile (NPDE = −1.2816), median (NPDE = 0), and 90th percentile (NPDE = 1.2816). A, 7.4% were below 10th percentile, 50.8% above 50th percentile, and 6.2% above 90th percentile. B, 1.5% were below 10th percentile, 17.0% above 50th percentile, and 3.6% above 90th percentile. C, 3.3% were below 10th percentile, 50.9% above 50th percentile, and 8.6% above 90th percentile. IP-10 indicates interferon-$\gamma$–induced protein 10; NPDE, normalized probability distribution error.

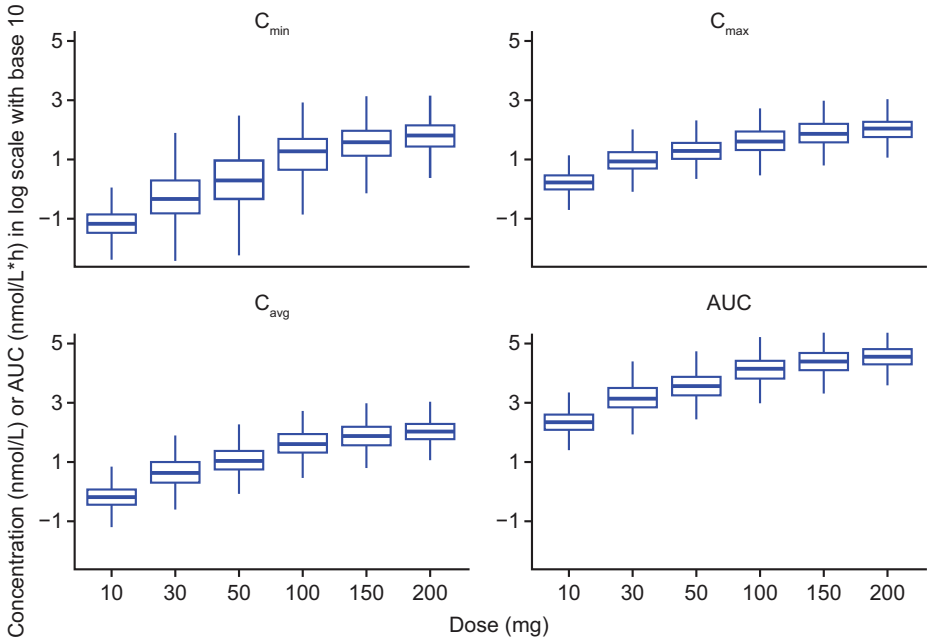


**Figure 3.** Simulated exposure parameters at steady state. Y axis is in log scale with base 10. AUC indicates area under the curve; $C_{avg}$, average concentration; $C_{max}$, maximum concentration; $C_{min}$, minimum concentration.

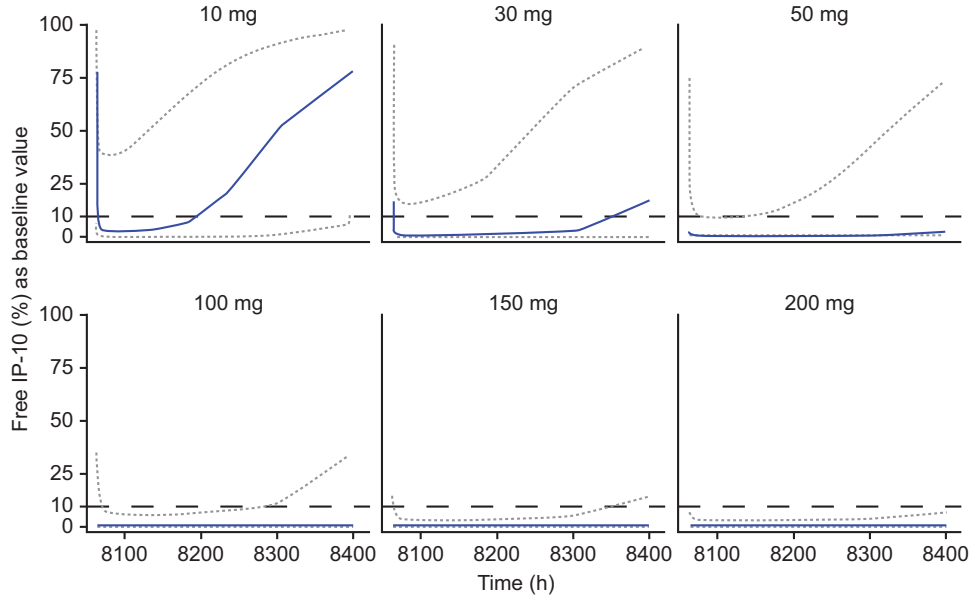


**Figure 4.** Simulated free IP-10 percentage as baseline value at steady state for each of the 6 SC Q2W dose panels. Solid line represents the median, and the dotted lines represent the 5% and 95% quantiles from the simulations. Dashed line at 10% represents the threshold for effective target suppression. IP-10 indicates interferon-$\gamma$–induced protein 10; Q2W, every 2 weeks; SC, subcutaneously.

during the SAD study. One participant in the placebo arm had an SAE (ventricular tachycardia) during the MAD study. The SAE resolved with treatment, and the participant was discontinued from the study. Four participants were discontinued due to AEs in the MAD study. One was due to the SAE mentioned, and 3 were due to nonserious AEs (vomiting; infusion-related reaction; peripheral swelling, myalgia, and arthralgia; all received BMS-986184). Two participants in the 200-mg Q2W group in the MAD study developed and sustained antidrug antibodies (ADAs) against BMS-986184. One participant developed ADAs on day 15, which were sustained until study discharge on day 85; the other participant developed ADAs on day 43, which were sustained until study discharge on day 86. No obvious differences in the drug, free IP-10, and total IP-10 profiles of these

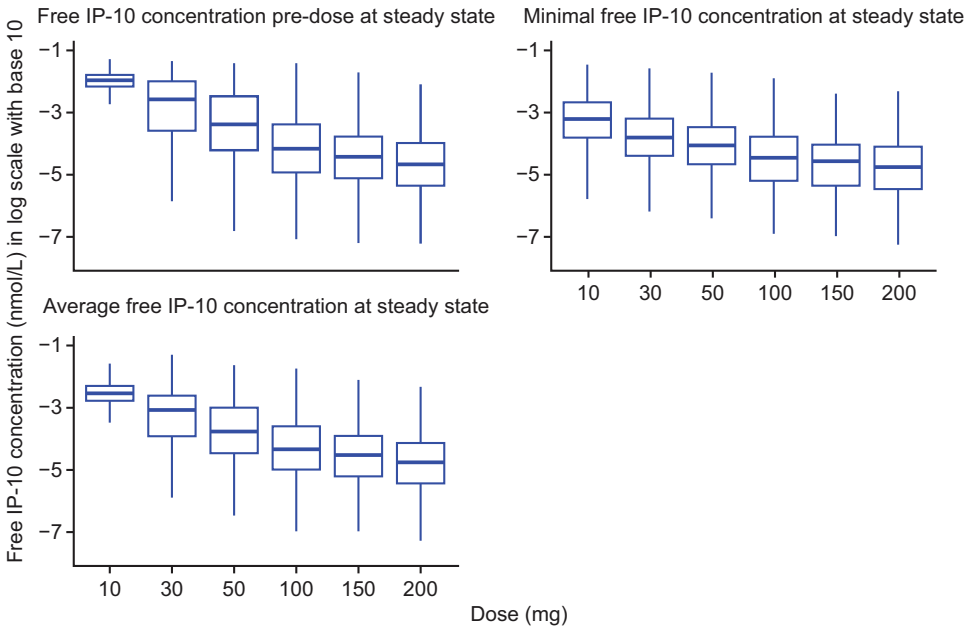


**Figure 5.** Simulated free IP-10 summary parameters at steady state. Y axis is in log scale with base 10. IP-10, interferon-$\gamma$–induced protein 10.

2 participants compared with other participants were observed by visually checking.

## Discussion

A 2-target TMDD structural model with QSS assumption and stimulation of IP-10 production was developed to characterize PK and TE of BMS-986184 in healthy participants by simultaneous fitting of the drug, free IP-10, and total IP-10 data. The results and predictions showed that the model fit reasonably well for the drug, free IP-10, and total IP-10 concentration data in the FIH study. The TMDD model was then used to conduct simulations of a virtual population of healthy individuals to predict PK and TE responses for different dosage regimens. Here, we demonstrate that a dose of approximately 150 mg Q2W could be a suitable dosage regimen for future clinical trials. BMS-986184 was generally well tolerated at the doses studied.

It is important to note that the approach here has a more mechanistic focus, rather than a clinical focus. Integrated modeling strategies, such as the one described here, provide a mechanistic framework for understanding and extrapolating PK and dose across different populations and disease states. The use of these models has the potential to increase the efficiency of drug development, reduce the need for animal studies, and increase PK understanding.[30] A QSS model was selected to characterize BMS-986184, as this model has the ability to accurately predict the phase in which the amount of receptor available is close to 0,[24] which represents the majority of our data points.

**Table 3.** Fraction of the Dose Elimination Via Different Elimination Routes

| Dose (mg) | Fraction of Linear Elimination | Fraction of IP-10 Elimination | Fraction of MM Elimination |
|---|---|---|---|
| 10 | 0.074 | 0.334 | 0.558 |
| 30 | 0.196 | 0.211 | 0.548 |
| 50 | 0.322 | 0.170 | 0.470 |
| 100 | 0.553 | 0.123 | 0.300 |
| 150 | 0.663 | 0.102 | 0.212 |
| 200 | 0.744 | 0.084 | 0.160 |

IP-10 indicates interferon-$\gamma$–induced protein 10; MM, Michaelis-Menten. Because the median of the fraction of elimination was used, the total of 3 fractions of elimination via different elimination routes is not necessarily equal to 100%.

The final model indicated the possible contribution of an unobserved second target (MIG/CXCL9) to the drug elimination; this contribution was described by the MM elimination term. The MM constant of target-mediated drug elimination from the central compartment ($K_m$) of this term was estimated to be 3 orders of magnitude (1443 times) higher than the $K_D$ of the drug-target complex, in agreement with similar differences in the $K_D$ of the drug binding to MIG/CXCL9 and IP-10, respectively (data on file, BMS investigators' brochure). It is difficult to estimate model parameters related to the unobservable target.[27] To improve model convergence and stability for the analysis data, variance for maximum target-mediated drug elimination rate from

the central compartment in MM function and $K_m$ were fixed to small values. Thus, the TMDD model developed in this study was able to account for both high-affinity target (human IP-10 with a $K_D$ of <0.1 nmol/L) and low-affinity target (MIG/CXCL9 with a $K_D$ of 200 nmol/L; data on file, BMS investigators' brochure).

Parameter estimates demonstrated that the central and peripheral compartments had similar volumes and yielded a total volume of distribution of around 7 L; however, it is important to note the high variance in the estimates for peripheral compartment volume. As evident from Table 3, linear elimination is dominant at the highest dose level, whereas at the lowest dose level almost all drug is eliminated by the target-mediated pathways. At all dose levels the MM elimination fraction (possibly related to MIG/CXCL9 binding) is 2 to 3 times larger than the fraction of the dose eliminated by the IP-10–mediated pathway. Both target-mediated pathways contribute to the overall elimination, allowing estimation of the target-related model parameters with reasonable precision.

A function of stimulation of the free IP-10 target production by the drug concentration was added to replicate stimulation of IP-10 production by IFN-$\gamma$.[11] This assumption considers the possible flux of IP-10 from tissue to circulation so that it would act as if the production of IP-10 were increased by drug treatment. It is possible that the addition of dose as a covariate in the stimulated production function in our model may explain the discrepancies seen between the physiologic free IP-10 data and the results of the model (Figure 1).

A few limitations of this model must be considered. Duration of dosing was short, with participants receiving a maximum of 2 doses. As a result, issues may arise in extrapolating steady-state data based on this limited data set. In addition, model development was based on the data from healthy participants in this FIH study, with no UC patient data as a validation data set. Because the levels and production of IP-10, as well as its interaction with BMS-986184, may be different in patients with UC compared with healthy participants, dosage projections for patients with UC must be approached with caution. Finally, it should be noted that clearance of mAbs is typically faster in patients with UC than in healthy volunteers,[31,32] and thus consideration must be taken when selecting therapeutic doses for patients.

## Conclusions

The use of a model-based approach allowed the characterization of the PK and TE of BMS-986184 in healthy participants. Integrated modeling strategies such as this can be used to help guide rational drug development by narrowing the possibilities regarding doses and schedules to be tested in clinical trials.

## Acknowledgments

This study was sponsored by Bristol-Myers Squibb. Professional medical writing and editorial assistance was provided by Lola Parfitt, MRes, at Caudex and was funded by Bristol-Myers Squibb.

## Disclosures

W.C., T.L., M.K., H.Z., H.G., J.T., S.B., and I.G. are employees of Bristol-Myers Squibb. The study was sponsored by Bristol-Myers Squibb. L.G. is a paid consultant of Bristol-Myers Squibb. H.S. is a former employee of Bristol-Myers Squibb.

## Author Contributions

All authors made substantial contributions to the conception and design, execution, or analysis and interpretation of data for this study. All authors were involved in writing and critically drafting the article or revising it critically for important intellectual content. All authors approved the final version to be submitted for publication and agree to be accountable for all aspects of the work. All authors had full access to all data in the study and take responsibility for the integrity of the data and the accuracy of the data analysis.

## References

1. Hanaoka R, Kasama T, Muramatsu M, et al. A novel mechanism for the regulation of IFN-$\gamma$ inducible protein-10 expression in rheumatoid arthritis. *Arthritis Res Ther*. 2003;5(2):R74-R81.
2. Kong KO, Tan AW, Thong BYH, et al. Enhanced expression of interferon-inducible protein-10 correlates with disease activity and clinical manifestations in systemic lupus erythematosus. *Clin Exp Immunol*. 2009;156(1):134-140.
3. Antonelli A, Ferrari SM, Corrado A, Ferrannini E, Fallahi P. CXCR3, CXCL10 and type 1 diabetes. *Cytokine Growth Factor Rev*. 2014;25(1):57-65.
4. Liu M, Guo S, Stiles JK. The emerging role of CXCL10 in cancer (review). *Oncol Lett*. 2011;2(4):583-589.
5. Lang S, Li L, Wang X, et al. CXCL10/IP-10 neutralization can ameliorate lipopolysaccharide-induced acute respiratory distress syndrome in rats. *PLoS One*. 2017;12(1):e0169100.
6. Lee EY, Lee Z-H, Song YW. CXCL10 and autoimmune diseases. *Autoimmun Rev*. 2009;8(5):379-383.
7. Corrado A, Mazzi V, Ferrari SM, et al. [Cryoglobulinemia and the $\alpha$-chemokine IP-10] (Article in Italian). *La Clinica terapeutica*. 2014;165(4):e317-e322.

8. Dyer KD, Percopo CM, Fischer ER, Gabryszewski SJ, Rosenberg HF. Pneumoviruses infect eosinophils and elicit MyD88-dependent release of chemoattractant cytokines and interleukin-6. *Blood*. 2009;114(13):2649-2656.
9. Luster AD, Ravetch JV. Biochemical characterization of a gamma interferon-inducible cytokine (IP-10). *J Exp Med*. 1987;166(4):1084-1097.
10. Lunardi S, Lim SY, Muschel RJ, Brunner TB. IP-10/CXCL10 attracts regulatory T cells: implication for pancreatic cancer. *Oncoimmunology*. 2015;4(9):e1027473.
11. Liu M, Guo S, Hibbert JM, et al. CXCL10/IP-10 in infectious diseases pathogenesis and potential therapeutic implications. *Cytokine Growth Factor Rev*. 2011;22(3):121-130.
12. Mayer L, Sandborn WJ, Stepanov Y, et al. Anti-IP-10 antibody (BMS-936557) for ulcerative colitis: a phase II randomised study. *Gut*. 2014;63(3):442-450.
13. Antonelli A, Ferrari SM, Giuggioli D, Ferrannini E, Ferri C, Fallahi P. Chemokine (C–X–C motif) ligand (CXCL)10 in autoimmune diseases. *Autoimmun Rev*. 2014;13(3):272-280.
14. Suzuki K, Kawauchi Y, Palaniyandi SS, et al. Blockade of interferon-$\gamma$-inducible protein-10 attenuates chronic experimental colitis by blocking cellular trafficking and protecting intestinal epithelial cells. *Pathol Int*. 2007;57(7):413-420.
15. Sasaki S, Yoneyama H, Suzuki K, et al. Blockade of CXCL10 protects mice from acute colitis and enhances crypt cell survival. *Eur J Immunol*. 2002;32(11):3197-3205.
16. Zhao Q, Kim T, Pang J, et al. A novel function of CXCL10 in mediating monocyte production of proinflammatory cytokines. *J Leukoc Biol*. 2017;102(5):1271-1280.
17. Kamath AV. Translational pharmacokinetics and pharmacodynamics of monoclonal antibodies. *Drug Discov Today Technol*. 2016;21-22:75-83.
18. Mould DR, Green B. Pharmacokinetics and pharmacodynamics of monoclonal antibodies: concepts and lessons for drug development. *BioDrugs*. 2010;24(1):23-39.
19. Rosario M, Dirks NL, Gastonguay MR, et al. Population pharmacokinetics-pharmacodynamics of vedolizumab in patients with ulcerative colitis and Crohn's disease. *Aliment Pharmacol Ther*. 2015;42(2):188-202.
20. Gibiansky L, Gibiansky E. Target-mediated drug disposition model: approximations, identifiability of model parameters and applications to the population pharmacokinetic-pharmacodynamic modeling of biologics. *Expert Opin Drug Metab Toxicol*. 2009;5(7):803-812.
21. Wang W, Wang X, Doddareddy R, et al. Mechanistic pharmacokinetic/target engagement/pharmacodynamic (PK/TE/PD) modeling in deciphering interplay between a monoclonal antibody and its soluble target in cynomolgus monkeys. *AAPS J*. 2014;16(1):129-139.
22. Chen X, Jiang X, Jusko WJ, Zhou H, Wang W. Minimal physiologically-based pharmacokinetic (mPBPK) model for a monoclonal antibody against interleukin-6 in mice with collagen-induced arthritis. *J Pharmacokinet Pharmacodyn*. 2016;43(3):291-304.
23. Lowe PJ. Applying physiological and biochemical concepts to optimize biological drug development. *Clin Pharmacol Ther*. 2010;87(4):492-496.
24. Dua P, Hawkins E, van der Graaf PH. A tutorial on target-mediated drug disposition (TMDD) models. *CPT Pharmacometrics Syst Pharmacol*. 2015;4(6):324-337.
25. Mager DE, Krzyzanski W. Quasi-equilibrium pharmacokinetic model for drugs exhibiting target-mediated drug disposition. *Pharm Res*. 2005;22(10):1589-1596.
26. Gibiansky L, Gibiansky E, Kakkar T, Ma P. Approximations of the target-mediated drug disposition model and identifiability of model parameters. *J Pharmacokinet Pharmacodyn*. 2008;35(5):573-591.
27. Gibiansky L, Gibiansky E. Target-mediated drug disposition model for drugs that bind to more than one target. *J Pharmacokinet Pharmacodyn*. 2010;37(4):323-346.
28. Gibiansky L, Gibiansky E, Bauer R. Comparison of Nonmem 7.2 estimation methods and parallel processing efficiency on a target-mediated drug disposition model. *J Pharmacokinet Pharmacodyn*. 2012;39(1):17-35.
29. Bergstrand M, Karlsson MO. Handling data below the limit of quantification in mixed effect models. *AAPS J*. 2009;11(2):371-380.
30. Jones HM, Mayawala K, Poulin P. Dose selection based on physiologically based pharmacokinetic (PBPK) approaches. *AAPS J*. 2013;15(2):377-387.
31. Hua F, Ribbing J, Reinisch W, Cataldi F, Martin S. A pharmacokinetic comparison of anrukinzumab, an anti-IL-13 monoclonal antibody, among healthy volunteers, asthma and ulcerative colitis patients. *Br J Clin Pharmacol*. 2015;80(1):101-109.
32. Passot C, Mulleman D, Bejan-Angoulvant T, et al. The underlying inflammatory chronic disease influences infliximab pharmacokinetics. *MAbs*. 2016;8(7):1407-1416.

## Supplemental Information

Additional supplemental information can be found by clicking the Supplements link in the PDF toolbar or the Supplemental Information section at the end of web-based version of this article.